Article

A Multi-phase Mesoscopic Simulation Model for the Long-term Chloride ingress and Electrochemical Chloride Extraction

Xuandong Chen[1,2], Feng Fu[3], Hai Wang[4], Qiuqun Liang[5,*], Aiping Yu[2], Kai Qian[1], Ping Chen[2,6]

[1] College of Civil and Architecture Engineering, Guilin University of Technology, Guilin 541004, China.
[2] Guangxi Key Laboratory of New Energy and Building Energy Saving, Guilin 541004, China.
[3] School of Mathematics, Computer Science and Engineering, City, University of London, London, UK
[4] College of Materials Science and Engineering, Guilin University of Technology, Guilin 541004, China
[5] College of Science, Guilin University of Technology, Guilin, 541004, China.
[6] Guangxi Engineering and Technology Center for Utilization of Industrial Waste Residue in Building Materials, Guilin, 541004, China.
* Correspondence: liangqq@glut.edu.cn (Q.L).

Abstract: Electrochemical chloride extraction (ECE) is one of the effective methods to remove chloride and prolong the service life of reinforced concrete (RC) structures. To fully understand the mechanisms of the long-term chloride ingress and subsequent ECE treatment of RC structure, a multi-phase mesoscopic numerical model is proposed. Unlike most of existing models, the long-term chloride ingress and the effect of chloride binding are considered in the proposed model, and the transport of chloride is simulated through a novel diffusion-migration-reaction process. The numerical simulation results show that the adsorption capacity of concrete to chloride decreases with the increase of chloride ingress time. Interestingly, the free chloride concentration on the surface of concrete decreases dramatically, and the maximum value appears in the concrete protective cover after ECE treatment. Furthermore, ECE treatment time, current density and concrete protective cover have significant influences on ECE treatment efficiency. Besides, the quantitative relationship models between these factors and ECE treatment efficiency have been developed. Moreover, the use of stirrup can improve the efficiency of ECE treatment. The research outcomes reveal previously ignored fundamental aspects of the ECE treatment and provide insights for the durability prediction of RC structures.

Key words: Electrochemical chloride extraction; Chloride ingress; Ions migration; Reinforced concrete

1 Introduction

Reinforced concrete (RC) is the most widely used building material in the construction industry [1,2]. The combination of reinforcement and concrete makes full use of their advantages in mechanical properties. However, reinforcement corrosion in RC structures caused by chloride ingress is one of the most serious problems in marine engineering [3,4]. In the process of RC casting, passive film is formed around the surface of reinforcement in alkaline environment, which can effectively prevent the reinforcement from corroding [5–7]. Nevertheless, chloride in the marine environment diffuses into concrete through the pores of concrete [8,9] during the service life of RC structures. Once the chloride concentration around the surface of reinforcement reaches the critical chloride concentration, the passivation film of reinforcement will be destroyed, resulting in the corrosion of reinforcement, the crack of concrete protective cover, and finally the failure of the structure [10–12]. Therefore, it is essential to remove chloride from RC structures and prolong the service life of RC structures.

For decades, electrochemical repair methods play an important role in protecting the reinforcement embedded in concrete from corrosion [13-17]. Electrochemical repair methods include cathodic protection and electrochemical chloride extraction (ECE) [13–22]. The principle of cathodic protection is to prevent the reinforcement from corrosion by providing an appropriate cathodic polarization current for the reinforcement. [23–25]. Although cathodic protection can effectively inhibit the corrosion of reinforcement, it needs to use current in the whole service life of the RC structure, which requires a high cost [19,26].

Compared with cathodic protection, ECE has many advantages, such as convenient operation, low price and short duration. The ECE system applies an external electric field between the embedded reinforcement bar (as cathode) and the external electrode (as anode, immersed in an electrolyte solution).. The external electric field drives the chloride ions to the external anode of concrete, thus removing the chloride from concrete[21,22,27]. ECE treatment has been favored by many researchers since it was first adopted in experimental researches in 1970s. For instance, Fajardo *et al*. [28,29]carried out the ECE treatment experiments on cylindrical concrete samples containing chlorides. The experimental results demonstrated that chloride in RC could be effectively removed by ECE treatment. In addition, after ECE treatment, about 50% ~ 60% of chloride in concrete were removed, while various cations such as Na^+, K^+ and Ca^{2+} in the concrete pore solution gathered around the reinforcement [28,29]. The study of Garcés *et al*. [30] showed that the efficiency of ECE treatment was influenced by the distributions of reinforcement. Besides, the ECE treatment efficiency can be improved by using graphene as an auxiliary electrode, and the chloride concentration in concrete can be reduced by 70% after 8 weeks of ECE treatment [31]. Furthermore, the environmental temperature also affects the ECE treatment efficiency. When the temperature increased from 0℃to 20℃, the ECE treatment efficiency was improved by two times [4]. Moreover, Yeih *et al*. [31] found that stirrups could increase the efficiency of ECE treatment. However, after ECE treatment, the new cementitious phases containing rich concentrations of sodium, aluminum and potassium were formed. Moreover, the ECE accumulates locally high amounts of alkali ions that stimulate the alkali–silica reaction.

The above experimental studies demonstrate that ECE treatment can effectively remove chloride from concrete. However, concrete is a multiphase composite material composed of

aggregate, mortar and interface transition zone (ITZ) [9,32]. The process of the chloride transport in concrete, especially in ITZ, is difficult to be explored by experiments. In contrast, numerical simulations have great advantages in providing detailed information, such as ions transport trajectories and interactions between ions, potential distributions, and so on [33]. The process of ECE can be simulated by using Nernst-Planck equation or Nernst-Planck-Poisson equation[14–16, 31, 34, 35]. Through numerical simulations, Wang *et al*. [16] reported that the position of the anode played an important role in the ECE treatment. In addition, by considering the effects of ionic concentrations on the diffusion and migration of charged ions, Li *et al*. [14,15] presented a mathematical model for simulating ECE treatment. Moreover, the ECE treatment numerical model established by Castellote *et al*. [34] took into account the effect of hydrogen ions produced by electrolytic water on the diffusion properties of chloride. Furthermore, Liu *et al*. [33,35] established a mesoscopic numerical model of ECE treatment and regarded concrete as a multiphase material. And the effects of aggregate shape, boundary condition and double electric layer on ECE treatment efficiency were discussed in their work.

The chlorides in concrete can be divided into the free chlorides and the bound chlorides [36,37]. In the stage of chloride ingress, the pore structure of concrete adsorbs some of free chlorides and become bound chlorides, reducing the permeability of concrete to chloride ions [38–41]. While, in the stage of ECE treatment, some of bound chlorides are released and become free chlorides. Unfortunately, most of the existing models only consider the free chlorides, and ignore the bound chlorides during the process of ECE treatment [8,31,42]. More importantly, the actual RC structure is attacked by chloride in the marine environment, and chloride concentration is non-uniformly distributed in concrete[43]. The concentration of chloride decreases with the increase of the ingress depth of chloride [39,41,44]. However, most of the existing numerical models for ECE treatment simulation assume that the chloride concentration in concrete is uniformly distributed before ECE treatment[14,21,45,46]. Obviously, this is not consistent to the real situation, and cannot fully reveal the mechanism of ECE treatment.

To tackle aforementioned problems, in this paper, a multi-phase mesoscopic numerical model is proposed to simulate the whole process of long-term chloride ingress and subsequent ECE treatment. In the proposed model, concrete is considered as a multiphase composite material composed of aggregate, mortar and ITZ. More importantly, by introducing a reaction phase, the binding effect of chloride ions is considered in the proposed model. In addition, the reliability of the proposed chloride model is verified by the third-part experiments. Furthermore, the distributions of chloride concentration in concrete are displayed in two-dimensional (2D) and three-dimensional (3D) graphics to reveal the evolution of chloride concentration distributions before and after ECE treatment. Moreover, the influences of ECE treatment time, current density, diameter of reinforcement and thickness of concrete protective cover on the efficiency of ECE treatment are discussed. And the quantitative relationship model between ECE treatment efficiency and these factors is presented. Finally, an engineering case is analyzed. The research outcomes reveal the previously overlooked aspects by other researchers in chloride transport mechanism in concrete meso-structure under the ECE treatment and provide insight for the durability prediction of RC structure subjected to chloride attack.

2 Theoretical background

2.1 Chloride ingress

In the marine environment, chloride mainly diffuses into the RC structure through the pore solution of the concrete, leading to the deterioration of the performance of RC structure. However, the diffusion of chloride in concrete pore solution is quite different from that in ordinary solution (e.g., water). When the external chlorides diffuse into the concrete, part of the free chlorides will become bound chlorides through the physical and chemical reactions, as shown in Fig. 1. On the one hand, the pore structures of concrete have adsorption effect on chlorides [36,37]. Once the chloride in the pore solution gets close to the C-S-H gel wall, some of the free chlorides will be adsorbed, which is called physically bound chloride(adsorption), as shown in Fig. 1. Physical binding is a long process and reversible [44]. On the other hand, some chloride ion reacts with mineral composition of concrete (i.e., residual aluminates, sulfoaluminate phases) to form Friedel's salt ($C_3A{\cdot}CaCl_2{\cdot}10H_2O$) [36,37,44]. This chemical reaction process is called chemically binding and is generally considered to be instantaneous. The chlorides in chemical reaction are called chemically bound chlorides. Generally, the chloride ion is continuously diffused into the concrete. However, the amount of the mineral composition of concrete (*i.e.*, residual aluminates, sulfoaluminate phases) is constant [36,44]. Therefore, the concentration of the chemically bound chloride is independent of the free chloride concentration and only dependent of the amount of the mineral composition of concrete. And the chemically bound chloride is constant as the concentration of free chloride increases (as shown in Fig. 2). In addition, various chloride adsorption models [38–41] have been proposed to describe the complex chloride binding phenomenon. And the relationship between free chloride and bound chloride can be demonstrated in Fig. 2.

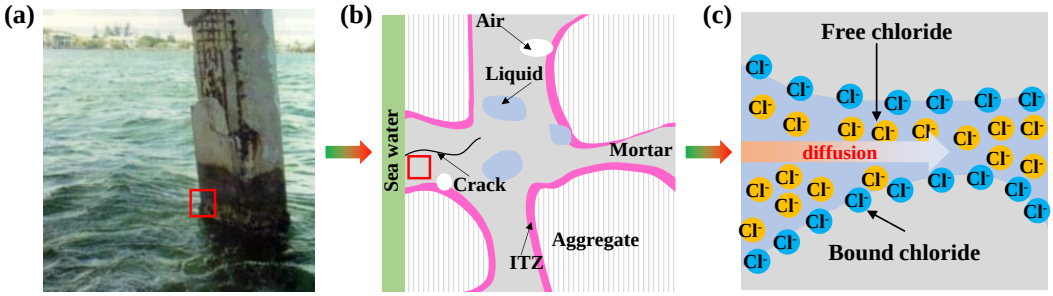

Fig. 1. Multi scale diffusion schematics of chloride ions. (a) Reinforced concrete column in marine environment [67]. (b) Multiphase composite structure of concrete. (c) Micro diffusion process of chloride.

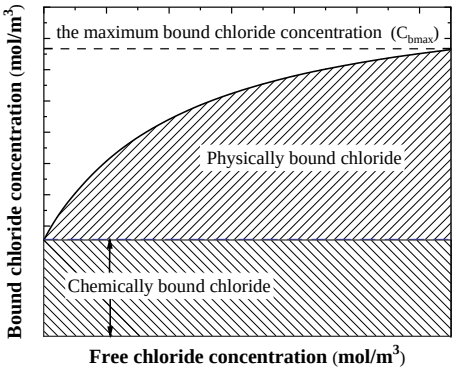

Fig. 2. Illustration of physically bound chloride and chemically bound chloride [44].

In addition, both the chemical binding and the physical binding can be regarded as a specific "reaction" of free chloride[48]. Consequently, the transport of chloride into concrete in the marine environment is essentially a diffusion-adsorption process. Without considering the electric field and the flow field, the governing equation of diffusion-adsorption of chloride can be expressed by the mass conservation equation as follows [48]:

$$\frac{\partial C_{cl}}{\partial t} = D_{cl}\frac{\partial^2 C_{cl}}{\partial x^2} + D_{cl}\frac{\partial^2 C_{cl}}{\partial y^2} - k_b\frac{C_{cl}}{C_{bmax}}(c_{bmax} - c_{cl}) \quad (1)$$

$$\frac{\partial C_b}{\partial t} = k_b\frac{C_{cl}}{C_{bmax}}(c_{bmax} - c_{cl}) \quad (2)$$

where C_{cl} is the free chloride concentration (mol/m^3), D_{cl} is the effective chloride diffusion coefficient (m^2/s), k_b is adsorption rate of bound chloride, C_b is the bound chloride concentration (mol/ m^3), and C_{bmax} is the maximum concentration of bound chloride (mol/m^3).

2.2 Electrochemical chloride extraction

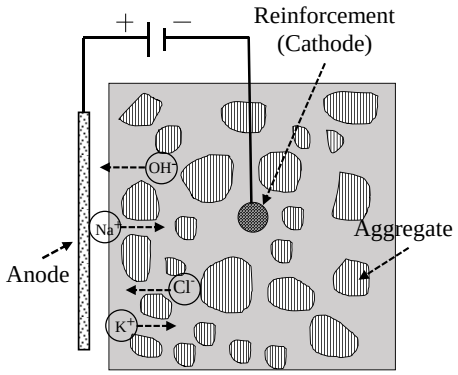

Fig. 3. Schematic representation of ECE treatment for concrete.

ECE is a process of directional movement of ions in concrete by applying an external electric field[21,22]. In the process of ECE, the cation ions move towards the positive electrode, while the anion ions move towards the surface of reinforcement embedded in concrete [4], as schematically illustrated in Fig. 3. Generally, the steel mesh immersed in the anode electrolyte is used as the positive electrode[28], and the reinforcement embedded in the concrete is used as the negative electrode[49,50]. In order to improve the conductivity of anodic system, in this paper, electrolyte solution with 50 mol/m^3 NaOH, 10 mol/m^3 LiOH and 5 mol/m^3 KOH is used. Under the external electric field, the transport of various ions in concrete is not only the diffusion of ions caused by the concentration gradient, but also the migration of ions caused by the potential difference. Based on the conservation of mass, hence, the transport of various ions in concrete can be expressed as follow[15,34,51]:

$$\frac{\partial C_i}{\partial t} = -\nabla J_i + k_{i_R}\frac{C_b}{C_{bmax}}(C_{iECE} - C_i) \quad (3)$$

where J_i is the molar flux of the i^{th} ionic species in the concrete ($mol/(m^2 \cdot s)$), C_{iECE} is ionic concentration at the beginning of ECE treatment, and k_{iR} is the release rate of the bound ions of the i^{th} ionic species.

The molar flux of ions per unit area per unit time can be expressed by Nernst-Planck equation[5]:

$$J_i = -D_i \nabla C_i - z_i D_i C_i \left(\frac{F}{RT} \nabla \phi\right) \quad (4)$$

where z_i is the charge number of the i^{th} ionic species, F = 96480 is the Faraday constant (C/mol), T = 298 is the absolute temperature (K), and R = 8.134 is the ideal gas constant (J/(mol·K)).

Substituting Eq. (4) into (3), it can yield the following equation:

$$\frac{\partial c_i}{\partial t} = D_i \nabla^2 c_i + \frac{z_i D_i F}{RT} \nabla (c_i \nabla \phi) + k_{iR} \frac{c_b}{c_{bmax}(c_{iECE} - c_i)} \quad (5)$$

According to the electric neutrality and current conservation, it yields [15,16,20,22]:

$$\sum_{i=1}^{N} z_i C_i = 0 \quad (6)$$

$$I = F \sum_{i=1}^{N} z_i J_i \quad (7)$$

where I is the current density (A/m^2).

Substituting Eq. (4) into (7), we have

$$\frac{F}{RT} \nabla \phi = -\frac{I/F + \sum_{i=1}^{N} z_i D_i \nabla C_i}{\sum_{i=1}^{N} z_i^2 D_i C_i} \quad (8)$$

It is worth to mention that the boundary conditions and initial conditions should be given in the simulations when calculating the concentration distribution of various ions in concrete. Under the external electric field, electrochemical reactions occur at the cathode and anode electrodes[21]. For the cathode, the oxygen absorption and the hydrogen evolution reactions occur on the surface of reinforcement embedded in the concrete [17]. And the chemical reactions at the cathode can be express as follows:

$$2H_2O + O_2 + 4e^- = 4OH^- \quad (9)$$

$$2H_2O + 2e^- = 4OH^- + H_2 \quad (10)$$

From Eq. (9) and (10), it is known that only OH^- ions are generated on the surface of reinforcement embedded in the concrete, and the flux of all the other ions is zero. Hence, the flux of OH^- on the surface of reinforcement embedded in the concrete is equal to the externally applied current density[28,49,51]:

$$J_{OH^-} = \frac{I_c}{z_{OH^-} \cdot F} \quad (11)$$

where I_c is the current density externally applied to the cathode.

Note that the volume of the anode electrolyte is quite large compared with that of the concrete pore solution, and the anode electrolyte is regularly replaced in the actual ECR treatment. Consequently, although the chlorides in the concrete transport to the anode electrolyte, the variation of ions concentration in anode electrolyte can still be ignored [52]. Therefore, in the simulation of ECE treatment process, the ions concentration in the anode electrolyte could be conservatively assumed to be constant[15]. And the initial values and boundary conditions used in the simulation of ECE treatment process are shown in Table 1.

Table1

Initial and boundary conditions in the simulation of ECE treatment [15,45,53–55].

Ions	Boundary concentration (mol/m^3)	Initial concentration (mol/m^3)	Charge number
Chloride	10	$C_{cl}(x, y, t_c)^*$	-1
Hydroxide	50	398.1	-1
Potassium	5	227.1	+1
Sodium	55	136.6	+1

*$C_{cl}(x, y, t_c)$ refers to the concentration of chloride in concrete in the t_c th year of chloride ingress.

2.3 Effective diffusion coefficient of various ions

As can been seen from Eq. (1) and (5) that the diffusion speed of ions in concrete is determined by the diffusion coefficient of ions. According to the diffusion theory for porous media, the effective specified ion diffusion coefficient in concrete can be calculated by the porosity, tortuosity and constrictivity of concrete[56], which can be expressed by

$$D_i = D_{s,i}\frac{\varphi\cdot\delta}{\lambda}\left(\frac{t_{ref}}{t}\right)^m \tag{12}$$

where $D_{s,i}$ is diffusion coefficient of the specified i^{th} ion in aqueous solution (m^2/s), ε is the porosity of concrete, δ is constrictivity of concrete, λ is tortuosity of concrete, t_{ref} is reference time (28d), t is chloride ingress, and m is the time attenuation index of chloride diffusion coefficient.

2.4 ECE treatment efficiency indexes

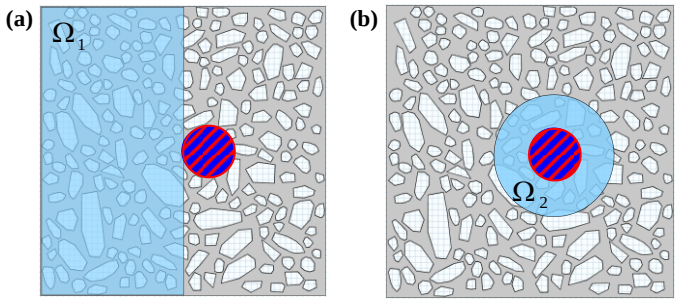

Fig. 4. Schematic representation of integral domains. (a) The integral domain of the concrete protective cover Ω_1. (b) The integral domain close to the reinforcement Ω_2.

The purpose of ECE treatment is to remove chloride ions from concrete as much as possible, especially region close to the surface of reinforcement [13]. In order to evaluate the effect of ECE treatment, the efficiency indexes of ECE treatment (i.e., P_1 and P_2) are defined. One of the ECE treatment efficiency indexes (P_1) is used to describe to the reduction of chloride concentration in the concrete protective cover domain, and the other efficiency index (P_2) is used to describe the reduction of chloride concentration in the region around the reinforcement, as shown schematically in Fig. 4a and b, respectively.

$$P_1 = \frac{\int_{\Omega_1} C(x,y,t_c)dA - \int_{\Omega_1} C(x,y,t_R)dA}{\int_{\Omega_1} C(x,y,t_c)dA} \tag{13}$$

$$P_2 = \frac{\int_{\Omega_2} C(x,y,t_c)dA - \int_{\Omega_2} C(x,y,t_R)dA}{\int_{\Omega_2} C(x,y,t_c)dA} \tag{14}$$

where P_1 and P_2 are efficiency indexes of ECE treatment, respectively; t_c is the moment when chloride concentration on the surface of reinforcement reaches critical chloride concentration; t_R

is the ECE treatment time; x and y are chloride position coordinates; A is the area; $C(x,y,t_R)$ is the free chloride concentration after ECE treatment; Ω_1 and Ω_2 are the integral domains, as shown in Fig. 4a and b, respectively.

3. Numerical simulations

In the numerical simulations, concrete is regarded as a multiphase composite material composed of aggregate, mortar matrix and ITZ, as schematically illustrated in Fig. 5a-b. In order to transform 3D concrete aggregate gradation into 2D concrete aggregate gradation, one of the widely applied aggregate distribution methods is Walraven's equation, which can be expressed as [9,57,58]:

$$P(d) = 1.065(d/d_m)^{1/2} - 0.053(d/d_m)^4 - (d/d_m)^6 - 0.0045(d/d_m)^8 - 0.0025(d/d_m)^{10} \quad (15)$$

where d is the diameter of aggregate; d_m is the maximum diameter of aggregates; $P(d)$ is the cumulative percentage passing a sieve with aperture diameter d.

In the proposed model, the shape of aggregate is random polygon, and the position of aggregate is also random. The diffusion coefficient of ions in aggregate is two orders of magnitude smaller than that in mortar matrix and ITZ [43]. Hence, the aggregate is regarded as impermeable body and the diffusion coefficient of ions in aggregate is set to be zero in the simulations. The thickness of ITZ is related to the construction technology, water/binder ratio and concrete curing conditions. Generally, the thickness of ITZ is between 20 *u*m and 100 *u*m [9,32,59]. In the proposed simulation model, the thickness of ITZ is random and obeys normal distribution, and the average thickness of ITZ is 60 *u*m. Fig. 5c shows the finite element mesh of the proposed numerical model, and there are more than 8 million degrees of freedom. Besides, all the other parameters used in the numerical simulation are listed in Table 2.

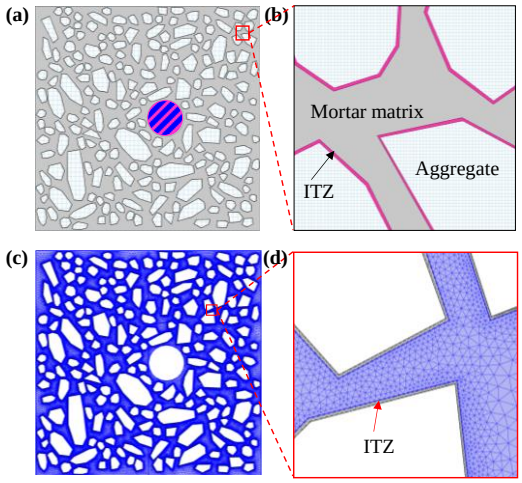

Fig. 5. Schematic of 2D multi-phase meso-structure of concrete. (a) Meso-structure of concrete. (b) Local magnification of the meso-structure. (c) Finite element mesh. (d) Local magnification of the finite element mesh

Table 2

Basic parameters in the numerical simulations.

No.	Parameters	Value	Unit	Meaning	References
1	D_{scl}	1.07×10^{-10}	m^2/s	Diffusion coefficient of chloride in solution	[15,21,22,45,46]
2	D_{sNa}	2.7×10^{-11}	m^2/s	Diffusion coefficient of sodium in solution	[15,21,22,45,46]
3	D_{sK}	3.9×10^{-11}	m^2/s	Diffusion coefficient of potassium in solution	[15,21,22,45,46]
4	D_{sOH}	5.28×10^{-10}	m^2/s	Diffusion coefficient of hydroxyl in solution	[15,21,22,45,46]
5	δc	0.75	--	Constrictivity of concrete mortar	[56]
6	τc	2	--	Tortuosity of concrete mortar	[56]
7	φc	12%	--	Porosity of concrete mortar	--
8	δ_{ITZ}	0.85	--	Constrictivity of ITZ	--
9	τ_{ITZ}	1	--	Tortuosity of ITZ	--
10	φ_{ITZ}	29%	--	Porosity of ITZ	--
11	m	0.2	--	Time attenuation index	[55]

A sodium chloride (NaCl) solution with a concentration of 471.8 mol/m^3 is set to the left side of the concrete to simulate marine environment. It's worth noting that only when the chloride concentration around the reinforcement surface reaches the critical chloride ion concentration, the ECE treatment is carried out by applying an external electric field. The flow chart of the derivation of the proposed multiphase numeric model is presented in Fig. 6

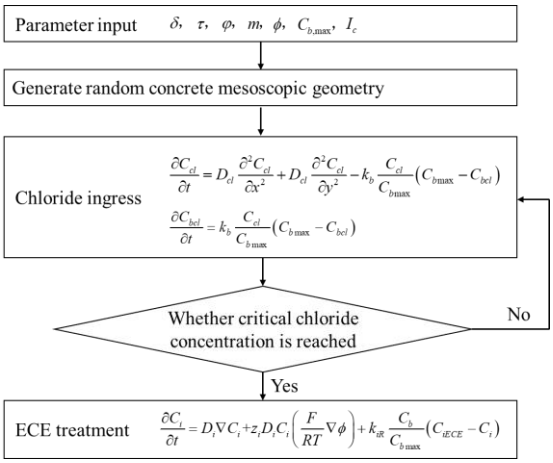

Fig. 6. The Flow chart of the chloride ingress and ECE treatment of the proposed multiphase numeric model.

In order to investigate the influence of current density, diameter of reinforcement, and thickness of concrete protective cover on the efficiency indexes (*i.e.*, P_1 and P_2) of ECE treatment, we calculate 24 different cases in the simulations, and the detailed parameters are listed in Table 3.

Table 3

Detailed parameters of each case.

Cases	Repair time (weeks)	Current density (A/m)	Thickness of concrete over (mm)	Diameter of reinforcement (mm)	Explications
Case 1	8	2	50	16	Benchmark Model
Case 2	1	3	50	16	Different treatment time
Case 3	2	3	50	16	
Case 4	3	3	50	16	
Case 5	4	3	50	16	
Case 6	5	3	50	16	
Case 7	6	3	50	16	
Case 8	7	3	50	16	
Case 9	8	3	50	16	
Case 10	8	0.5	50	16	Different current densities
Case 11	8	1	50	16	
Case 12	8	1.5	50	16	
Case 13	8	2.5	50	16	
Case 14	8	3	50	16	
Case 15	8	2	50	10	Different reinforcement diameters
Case 16	8	2	50	14	
Case 17	8	2	50	18	
Case 18	8	2	50	22	
Case 19	8	2	50	26	
Case 20	8	3	30	16	Different thicknesses of concrete protective cover
Case 21	8	3	35	16	
Case 22	8	3	40	16	
Case 23	8	3	45	16	
Case 24	8	3	50	16	

4. Model validation

The reliability of the model proposed in this paper can be verified by the measured data of chloride concentration in concrete by Wu *et al.* [55]. The test objects of the experiments were taken from Fangcheng port, Qinzhou port(as shown in Fig. 7), and Tieshan port in China [55]. A detailed description about the test objects, including construction time, building structure type and chloride ingress time, is presented in Table 4. The water/binder ratio of concrete for all the three ports is 0.4 and the concrete strength grade is C40. Additionally, the concrete powders were taken from the external wall of the structures in the in-situ test. When taking the sample from the ports, the drilling

depth was 56 mm and was divided into eight equal sections. The chloride concentration was measured by Rapid Chloride Concentration Tester (RCT). Here, we compare our simulation results of free chloride concentration in concrete with the experimental data, as demonstrated in Fig. 8a-c. Due to the randomness of aggregate distribution in concrete, the chloride concentration at the same ingress depth is slightly different. It is evident from Fig. 8a-c that the numerical simulation results are very close to the experimental data, implying that the proposed numerical model is reliable.

Fig. 7. Qinzhou port [55]

Table 4

Detailed description of the test objects.

No.	Dock	Built year	Structure types	Ingress time (months)
1	13# Dock of Fangcheng port	2005	Gravity type thin-walled cylindrical caisson structure	80
2	10# Dock of Qinzhou port	2008	The category of large cylinder gravity structure	62
3	1# Dock of Tieshan port	2009	The category of gravity caisson structure	35

Through the comparison of chloride concentration in concrete of splash region, tidal region and atmospheric region, it is obvious that the corrosion degree of RC structure of splash region is the most serious, as shown in Fig. 8a-c. This demonstrates that RC structure of Splash region is the first to fail in the marine environment. Therefore, it is of great significance to repair the RC structure of Splash region. In our work, the RC structure of Splash region is taken as the research object.

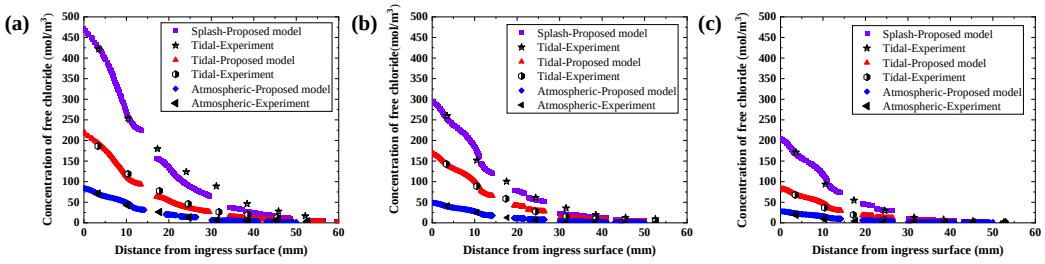

Fig. 8. Comparison of free chloride concentration between numerical results and experimental data. (a) Fangcheng port, (b) Qing zhou port, and (c) Tieshan port.

5. Results and discussions

5.1 Long-term chloride ingress simulations

The distribution of chloride concentration in concrete plays a vital role in evaluating the service performance of RC structure and judging whether the reinforcement is corroded or not [60,61]. Despite the continuous progress of experiments, it is time-consuming and costly to implement the long-term chloride ingress experiments[62]. And the long-term experiments with chloride ingress over 20 years have not been reported. However, for RC structures, the minimum service life required by the Code for Concrete Design is 50 years [68]. Therefore, it is significant to study the long-term chloride ingress process in RC structure, such as 25 years and 50 years of chloride ingress. To address these critical issues, herein, numerical simulation has been used to study the long-term chloride ingress process in RC structure and reveal the evolution process of chloride concentration.

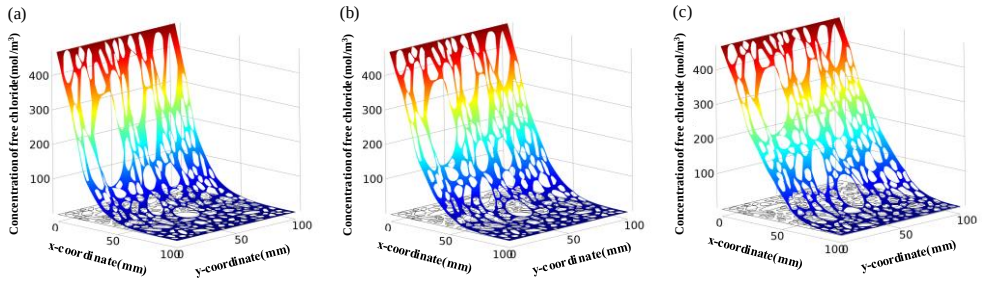

Fig. 9. Spatial distributions of free chloride at three different ingress times. (a) 10th year, (b) 25th year, and (c) 50th year, respectively.

In the experiments conducted by Wu *et al.* [55], the free chloride concentration in concrete of splash region of Fangcheng port was measured only after 80 months of chloride ingress. To better demonstrate the evolution process of chloride concentration in concrete, distributions of free chloride concentration at three different ingress times (*i.e.*, 10th year, 25th year, and 50th year) is investigated, as shown in Fig.9a-c. It should be mentioned that the diameter of reinforcement is 16 mm and the thickness of concrete protective cover is 50 mm in the simulation. The horizontal coordinates (*i.e.*, *x* and *y* coordinates) in Fig. 9a-c represent the coordinates of the concrete meso-structures, and the vertical coordinate (*i.e.*, *z* coordinate) represents the free chloride concentration. And the chloride erodes along the direction of *x*-axis. It is obvious from Fig. 9a-c that the free chloride concentration increases with the increases of chloride ingress time at the same ingress depth. This indicates that with the increase of ingress time, if no repair measures are taken, it will inevitably lead to the corrosion of reinforcement in RC structure. The spatial distributions of free chloride concentration in Fig. 9a-c could not only clearly reflect the evolution of chloride concentration, but also manifest the tortuosity effect of the chloride diffusion.

Additionally, the spatial distributions of bond chloride concentration at three different ingress times (*i.e.*, 10th year, 25th year, and 50th year) are demonstrated in Fig. 10a-c. It is apparent from Fig. 10a-c that the bound chloride concentration will not increase after reaching a stationary value, and the bound chloride reaches the saturation state. This indicates that the region where the bound

chloride reaches saturation state will no longer have the adsorption capacity of chloride and the adsorption capacity of concrete to chloride decreases with the increase of chloride ingress time.

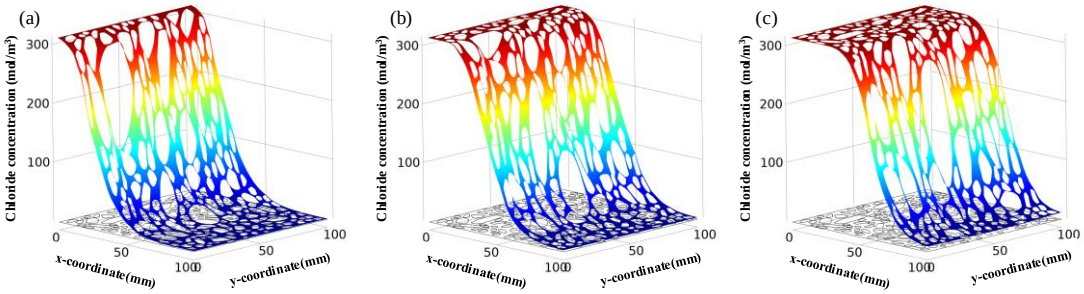

Fig. 10. Spatial distributions of bound chloride at three different times. (a) 10th year. (b) 25th year, and (c) 50th year, respectively.

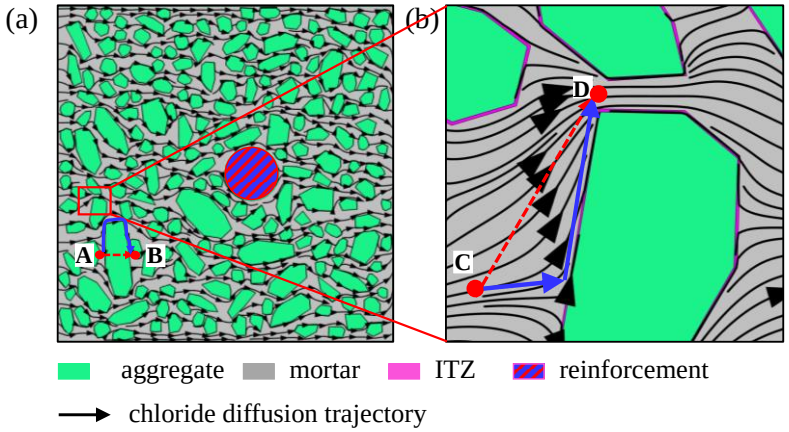

Fig. 11. Free chloride diffusion trajectories in meso-structures of concrete. (a) Overall concrete section (b) Local amplification.

The diffusion trajectories of chloride in the concrete meso-structures have been clearly presented in Fig. 11a-b. It is obvious from Fig. 11a-b that the aggregate increases the diffusion paths of chloride and hinders the diffusion of chloride. For example, in Fig. R11a, the chloride ions at point A cannot diffuse through the aggregate to point B along a straight line, but must diffuse around aggregate to point B, which significantly increases the diffusion path of the chloride ions. In order to study the influence of ITZ on chloride diffusion, Fig11 is partially enlarged. It is found that the chlorine ions at point C do not diffuse to point D along a straight line. Instead, the chlorine ions at point C diffuse first to the ITZ and then along the ITZ region to point D (as shown in Fig. 11B), indicating that ITZ is a fast channel for chlorine ion diffusion. This phenomenon has not been found in previous studies. Consequently, the mechanism of ITZ promoting the chloride diffusion in concrete can be well understood by this phenomenon. Moreover, the existence of random aggregates in concrete leads to the non-uniformity distribution of chloride concentration at the same ingress depth. This is quite different from the existing model [21] treating concrete as a single homogeneous material. In their models, the distribution of chloride concentration is uniform at the same ingress depth [21]. The proposed model with random distribution of aggregates is more consistent with the reality.

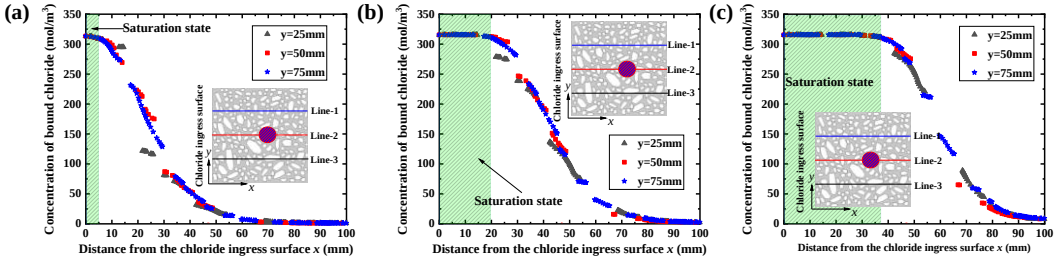

Fig. 12. The bond chloride profiles at three different ingress times. (a) 10th year. (b) 25th year, and (c) 50th year, respectively.

In order to further quantitatively study the distributions of chloride concentration in concrete, Fig. 12a-c shows how the bound chloride concentrations change with penetration depth at three different ingress times (*i.e.*, 10th year, 25th year, and 50th year). The simulation data of bound chloride concentration is extracted from the left to the right of the concrete at three random places inside the concrete (as shown in Fig. 12a-c by Line-1, Line-2, and Line-3). Obviously, due to the random distribution of aggerates in concrete, the data of three chloride concentration curves (Line-1, Line-2, and Line-3) are not completely coincident. It can also be seen from Fig. 12a-c that the saturated bound chloride region is gradually increasing with the increase of chloride ingress time. The depths of saturated bound chloride region are only 5 mm and 19.5 mm at 10th and 25th year of chloride ingress, respectively. However, it reaches to 37.2 mm at 50th year of chloride ingress.

Moreover, once the free chloride concentration on the surface of the reinforcement reaches the critical chloride concentration of 33.8mol/m^3[63–65], the reinforcement will begin to rust [65]. As can be seen from Fig. 13a, at 10th year of chloride ingress, the free chloride concentration on the surface of the reinforcement (*i.e.*, 13.2mol/m^3) is lower than the critical chloride concentration, and the reinforcement does not corrode at this stage. However, the free chloride concentration on the surface of the reinforcement (*i.e.*,33.8mol/m^3) has reached the critical chloride concentration at 25th year of chloride ingress (as showed in Fig. 13b), indicating that the reinforcement embedded in concrete begins to rust and the service life of RC structures is only 25 years. This is far lower than the service life required by Code for Concrete Design (*e.g.*, 50 years) [68]. To extend the service life of RC structures, it is necessary to take measures to remove chloride from concrete during the service life of the concrete. In the next section, the removal of chloride from concrete by ECE treatment will be described in detail.

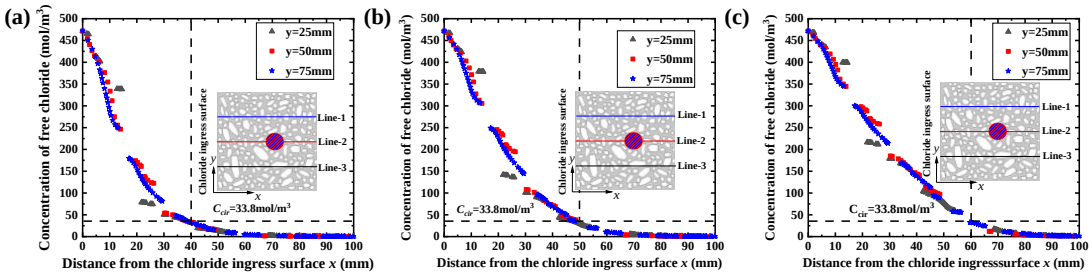

Fig. 13. The free chloride profiles at three different ingress times. (a) 10th year. (b) 25th year, and (c) 50th year, respectively.

5.2 ECE treatment simulations

The ECE method is adopted to remove chloride from concrete when the free chloride concentration on the surface of the reinforcement reaches the critical chloride concentration. Note that ECE treatment can significantly reduce chloride in RC structures in a very short period of time (usually 4~8 weeks) [29,66]. Therefore, the longest ECE treatment time in our simulation is 8 weeks. In the existing ECE treatment literatures, the distributions of chloride concentration in concrete were assumed to be uniform before ECE treatment, and the chloride concentration in concrete was set to be a constant, such as 380 mol/m^3 [14–16,33] or 200 mol/m^3 [22,66] and so on. However, this was not consistent with the actual situation.

In this section, the removal of chloride from concrete by ECE treatment is implemented at the 25th year of chloride ingress (as shown section 5.1). The current density applied to the reinforcement is 2 A/m^2, and the ECE treatment time is from 1 to 8 weeks with a step of one week. More detail information is presented in Table 3 (case 1 to case 8).

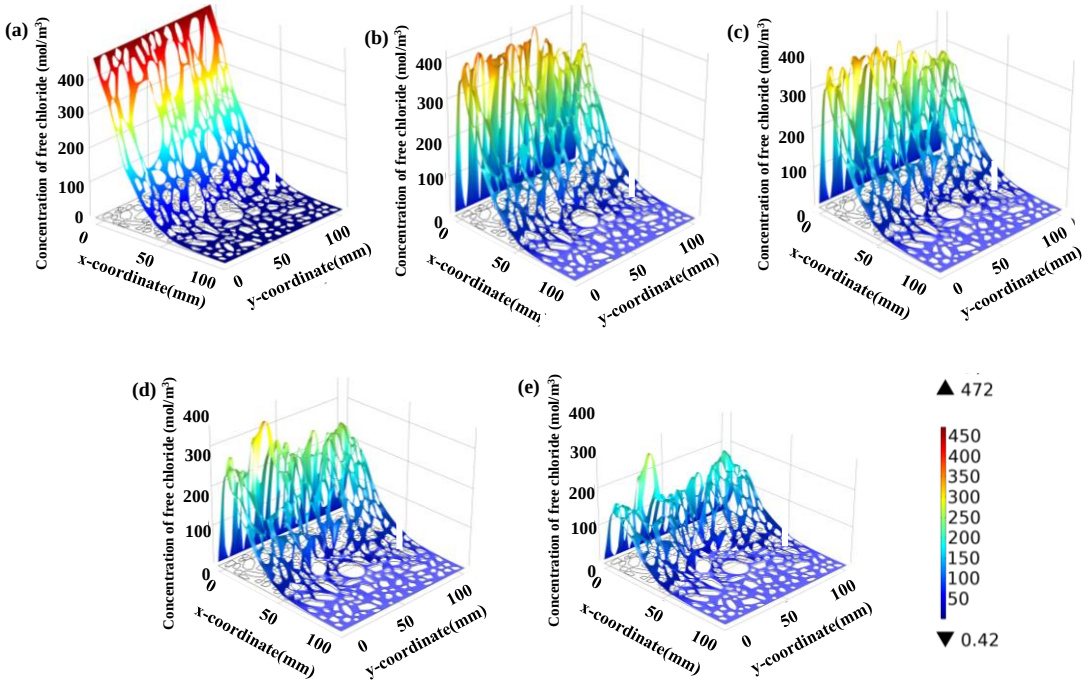

Fig. 14. Spatial distributions of free chloride concentration after different ECE treatment time. (a) Before ECE treatment. (b) After 1 weeks of ECE treatment. (c) After 2 weeks of ECE treatment. (d) After 4 weeks of ECE treatment. (e) After 8 weeks of ECE treatment, respectively.

The spatial distributions of free chloride concentration in RC structures after 1~8 weeks of ECE treatment have been calculated, as shown in Fig. 14b-e. For comparison, the spatial distributions of free chloride concentration in RC structures before ECE treatment is also presented in Fig. 14a. By comparing Fig. 14a and Fig. 14b, it is apparent that spatial distributions of free chloride concentration in RC structures changes dramatically after ECE treatment. Before the ECE treatment, the distribution of free chloride in the concrete decreases gradually as the ingress depth increases (as depicted in Fig.14a). However, after ECE treatment, the distribution of free chloride in the concrete first increases and then decreases with the increase of the ingress depth. This indicates that the maximum value of free chloride concentration appears inside the concrete after

ECE treatment (as depicted in Fig.14b-e), and not appears on the chloride ingress surface anymore (as shown in Fig.14a). This phenomenon has not been shown in the existing ECE treatment literatures[15,17,21,22,34]. More importantly, with the increase of ECE treatment time, the maximum value of free chloride concentration in concrete is significantly reduced, as shown in Fig14b-d, indicating that ECE method can effectively remove chloride in concrete.

Furthermore, Fig. 15a shows how the chloride concentrations change with increase of the ECE treatment times. It can be clearly seen from the Fig. 15a that with the increase of ECE treatment time, the maximum value of chloride concentration in concrete decreases, and the position of the peak is moving towards the interior of concrete. In addition, the chloride concentrations on the surface of reinforcement for different ECE treatment times have also been calculated, as shown in Fig. 15b. It is obvious from Fig. 15b that the chloride concentration on the surface of the reinforcement decreases sharply at the initial stage of ECR treatment, and then decreases gradually with the increase of desalting time. Similar results has also been found in the existing research work [17,21].

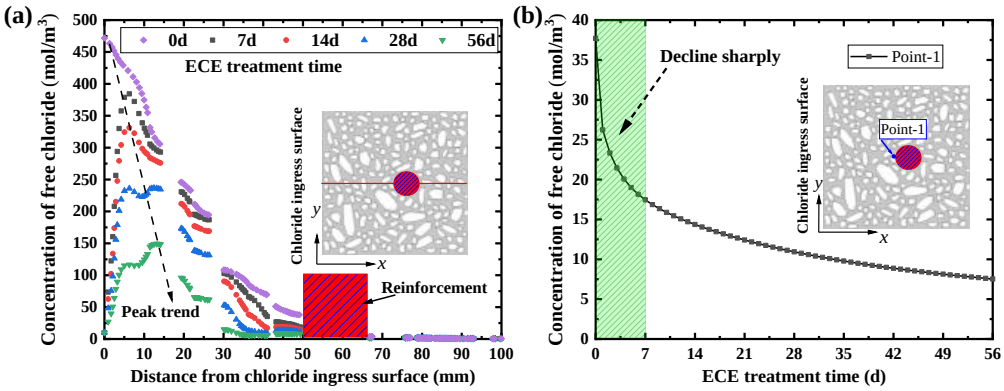

Fig. 15. Free chloride concentration profiles (a) at y = 50 mm with different ECE treatment time, (b) on the surface of reinforcement.

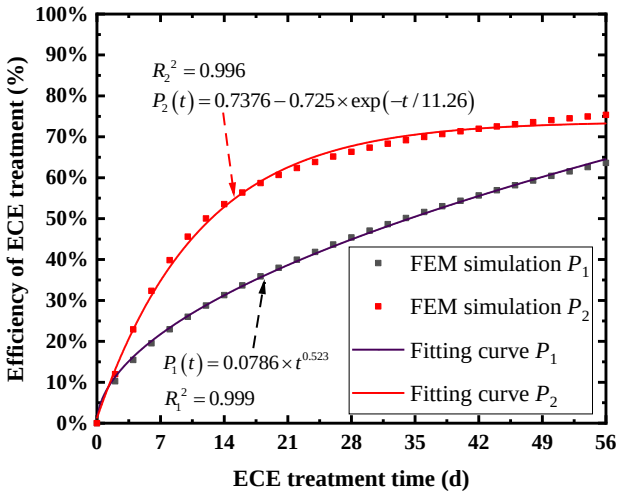

Fig. 16. Relationship curves between efficiency indexes (*i.e.*, P_1 and P_2) of ECE treatment and ECE treatment time.

In order to further quantitatively characterize the efficiency of ECE treatment, the efficiency indexes (*i.e.*, P_1 and P_2) of ECE treatment are calculated based on Eq. (13) and (14) and plotted in

Fig. 16. It can be apparent from the Fig. 16 that P_2 increase rapidly at first and then tends to be stable, and P_1 increase gradually with the increasing of ECE treatment time. In addition, the ECE treatment efficiency in concrete protective cover (P_1) is less than that around the reinforcement (P_2) for the same ECE treatment time. Moreover, after 8 weeks of ECE treatment, P_1 and P_2 have reached 63.6% and 75.4%, respectively. This also indicates that ECE treatment can effectively remove chloride from concrete.

Furthermore, the following formula fitted from the data of numerical simulation can be obtained by regression analysis, which can be used to describe the quantitative relationship between the efficiency indexes of ECE treatment and the ECE treatment time.

$$P_1(t) = 0.0786 \times t^{0.523} \quad (16)$$

$$P_2(t) = 0.7376 - 0.725 \times exp(-t/11.26) \quad (17)$$

where t denotes ECE treatment time (d).

5.3 Parametric analysis

To gain further insight into the efficiency of ECE treatment, the influence of some key factors (current density, diameter of reinforcement, and thickness of the concrete protective cover) on the efficiency of ECE treatment has been investigated.

5.3.1 Current density

The current density on the surface of reinforcement is one of the important factors affecting the efficiency of ECE treatment[33]. When the current density is too small, the efficiency of ECE treatment is reduced and the time of ECE treatment is prolonged [14,34]. To reveal the effect of current density on ECE treatment, ECE treatment of concrete with different current densities from 0.5 A/m^2 to 3 A/ m^2 have been investigated. Details are listed in Table 1 (*i.e.*, case 10 to case 14). Except for the current density, the simulation conditions from case 10 to case 14 are the same, which can eliminate the interference of other variables on the ECE treatment.

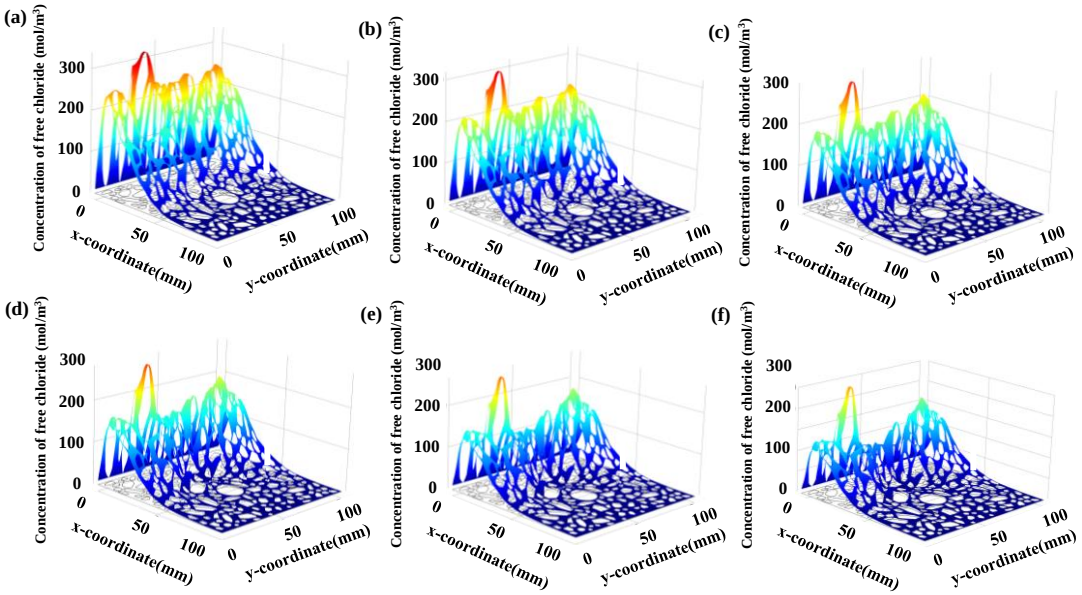

Fig. 17. Spatial distributions of free chloride concentration after 8 weeks of ECE treatment. (a) 0.5 A/m^2, (b) 1 A/m^2, (c) 1.5 A/m^2, (d) 2 A/m^2, (e) 2.5 A/m^2, and (f) 3 A/m^2, respectively.

After 8 weeks of ECE treatment, the distributions of free chloride concentration with different current densities are as shown in Fig. 17. Obviously, the overall characteristic spatial distributions

of free chloride concentration are consistent regardless of current density. For instance, all the peaks of free chloride concentration with different current densities are distributed between reinforcement and chloride ingress surface. This indicates that the current density of cathode does not change the distribution trend of free chloride concentration. However, with the increase of current density, the concentration of free chloride in concrete decreases gradually. It is worth noting that the current density on the surface of the reinforcement is proportional to the potential difference of the applied external electric field. A large potential difference will lead to a large current density. In addition, the migration rate of chloride in the electric field can be improved by increasing the potential difference according the Eq. (5). Therefore, large migration rate of chloride will mean that more chlorides will be removed from the concrete in the same repairing time, resulting a reduction of chloride concentration in concrete.

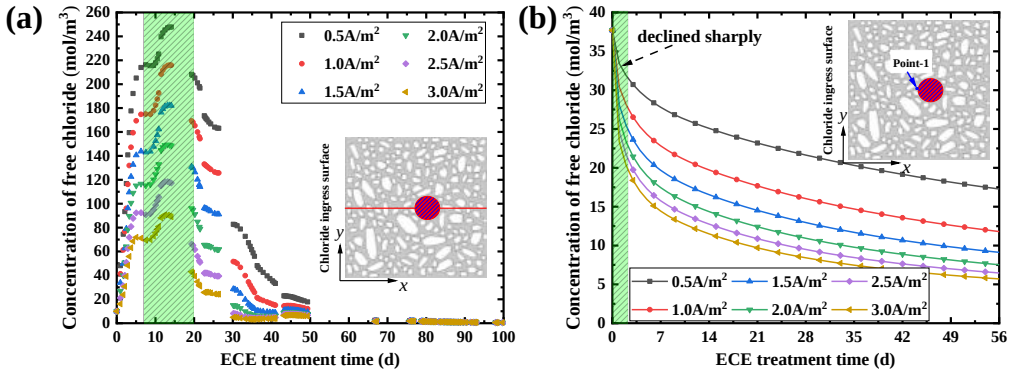

Fig. 18. Free chloride concentration profiles (a) at y = 50 mm, and (b) on the surface of reinforcement with different current density.

In order to quantitatively describe the effect of current density on ECE treatment, the distributions of free chloride concentration at y = 50 mm after 8 weeks of ECE treatment are calculated and demonstrated in. Fig. 18a. It reveals that with the increase of current density, the maximum value of chloride concentration is gradually decreasing. Besides, the peak position of chloride concentration is distributed between 8 mm and 20 mm away from the chloride ingress surface. Moreover, Fig. 18b shows the change curves of free chloride concentration on the surface of reinforcement with current densities. What stands out in this figure is the rapid decrease of the free chloride concentration in the initial stage of ECE treatment (0~3 days). In the later stage of ECE treatment, the free chloride concentration surrounding the reinforcement declines gradually. This is mainly due to that the chloride concentration around the reinforcement is very low in the later stage of ECE treatment.

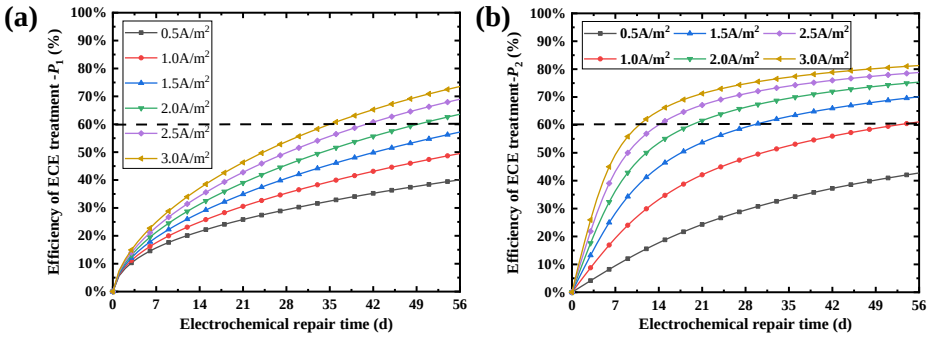

Fig. 19. Comparison of influences of different current densities on the efficiency indexes of ECE treatment. (a) The efficiency index P_1 of ECE treatment, (b) The efficiency index P_2 of ECE treatment.

Fig. 19a-b reveal that ECE treatment efficiency indexes P_1 and P_2 increase with the increase of current density. It is obvious from Fig. 19a-b that increasing current density can improve the removal of chloride ions at the same ECE time. Similar results have also been obtained from experimental researches conducted by Saraswathy *et al.* [67]. After 8 weeks of ECE treatment, the ECE treatment efficiency indexes P_1 and P_2 with current density of 2 A/m^2 are 63.6% and 73.2%, respectively. While the ECE treatment efficiency indexes P_1 and P_2 with current density of 3 A/m^2 after 8 weeks of ECE treatment are 75.3%, and 81.3%, respectively. However, with the increase of current density, the hydrogen generated on the surface of reinforcement is increasing. The hydrogen generated by ECE treatment will make the reinforcement brittle, which is not conducive to the overall performance of the RC structure [33]. Considering the damage of hydrogen to reinforcement, the optimized current density is 2 A/m^2.

In order to further reveal the relationship between current density and ECE treatment efficiency (*i.e.*, P_1 andP_2), the change trend of ECE treatment efficiency (*i.e.*, P_1 and P_2) with current density is shown in Fig. 20a-b. It can be clearly seen from Fig. 20a-b that with the increase of current density, P_1 increases linearly, and P_2 first increases and then stabilizes. Through regression analysis, the correlation between current density and the ECE treatment efficiency (*i.e.*, P_1 and P_2) can be express as follows:

$$P_1(i) = 0.1326 \times i + 0.356 \quad (18)$$

$$P_2(i) = -0.0723 \times i^2 + 0.397 \times i + 0.2625 \quad (19)$$

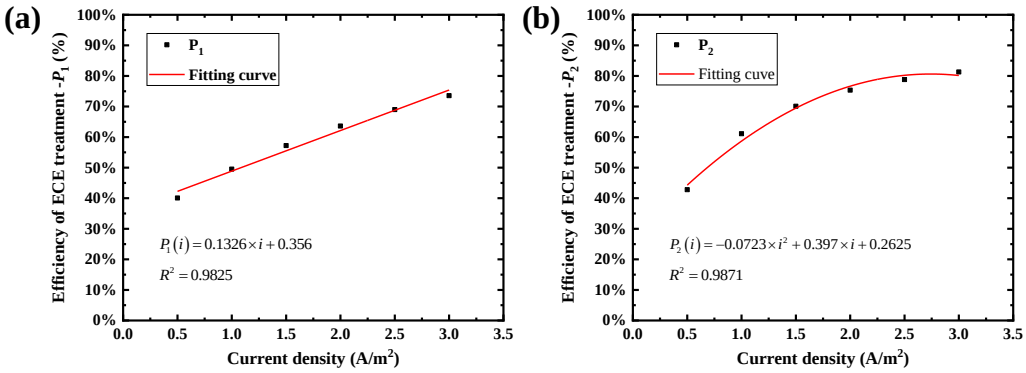

Fig. 20. The change trend of ECE treatment efficiency. (a) The efficiency index P_1 of ECE treatment, (b) the efficiency index P_2 of ECE treatment.

5.3.2 Diameter of reinforcement

In the process of ECE treatment, the reinforcement embedded in concrete is regard as the cathode electrode[26,31]. In marine engineering, the diameters of reinforcement used in different building structures are different[68,69]. However, the diameter of the reinforcement can directly affect the distribution of the electric field and the formation range of hydroxides [14,33]. Therefore, it is necessary to discuss the influence of reinforcement diameter on the ECE treatment. In this section, the ECE treatment of RC structures with different reinforcement diameters (*i.e.*, 10 mm, 14 mm, 18 mm, 22 mm and 26 mm) are simulated. And all the other parameters used in the simulations are listed in Table 1 (case 15 to case 19). It should be noted that the simulation conditions of case

15 to case 19 are the same, except for the diameter of the reinforcement, which can eliminate the interference of other variables on the ECE treatment.

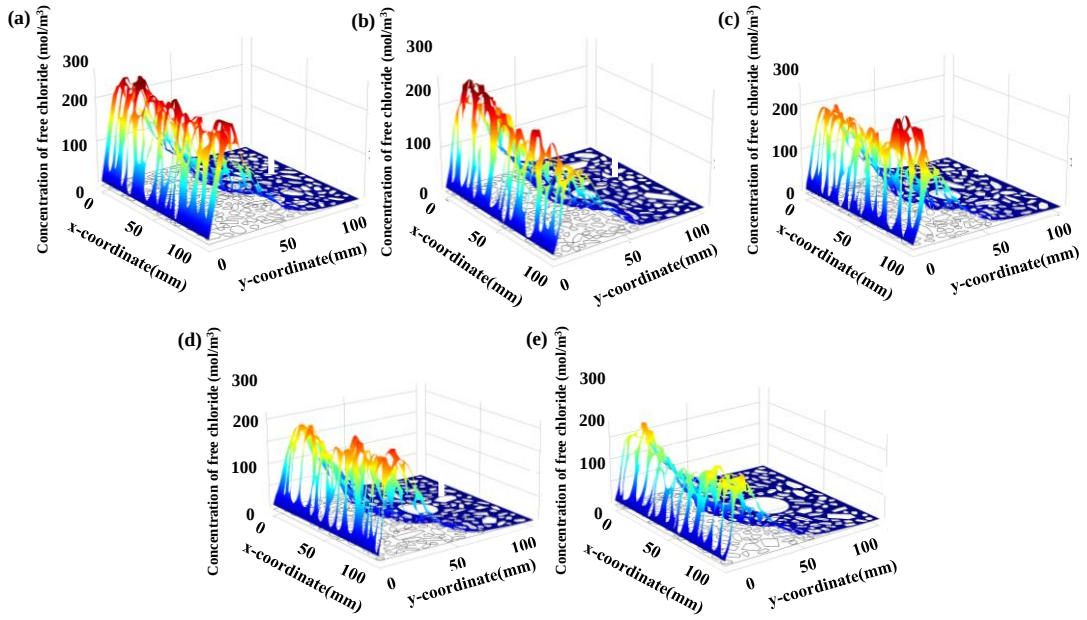

Fig. 21. Spatial distributions of free chloride concentration after 8weeks of ECE treatment for different diameters of the reinforcement. (a) ϕ =10 mm, (b) ϕ =14 mm, (c) ϕ =18 mm, (d) ϕ =22 mm, and (e) ϕ =26 mm, respectively.

The spatial distributions of free chloride concentration for different diameters of reinforcement after 8 weeks of ECE treatment are calculated, as shown in Fig. 21a-e. It is apparent from Fig. 21a-e that the free chloride concentration in the concrete gradually decreases with the increase of reinforcement diameter. It is worth noting that the reinforcement embedded in concrete is regard as the cathode electrode, and the cathode has a repulsive effect on chloride. With the increase of reinforcement diameter, the repulsive effect is more obvious. Hence, ECE treatment effect is getting better and better with the increase of reinforcement diameter. However, compared with the current density, the free chloride concentration does not decrease significantly with the increase of reinforcement diameter, and the reinforcement diameters had little effect on ECE treatment. compared with the current density.

In addition, the relationship between efficiency indexes (P_1 and P_2) of ECE treatment and reinforcement diameter are shown Fig. 22a and b. The ECE treatment index P_1 increases linearly with the increase of the reinforcement diameters, as depicted in Fig.22a. Through linear regression analysis, the quantitative relationship between them can be expresses as:

$$P_1(\phi) = 0.01393 \times \phi + 0.35382 \tag{20}$$

where ϕ is diameter of the reinforcement.

Fig 22b describes the histogram of the ECE treatment index P_2 with different reinforcement diameters. Obviously, with the increase of reinforcement diameter, the change of efficiency index P_2 of ECE treatment is trifling. The maximum value of P_2 is 76%, and the minimum value is 71% with a difference of only 5%. Therefore, the influence of reinforcement diameter on ECE treatment indexes of P_2 could be ignored.

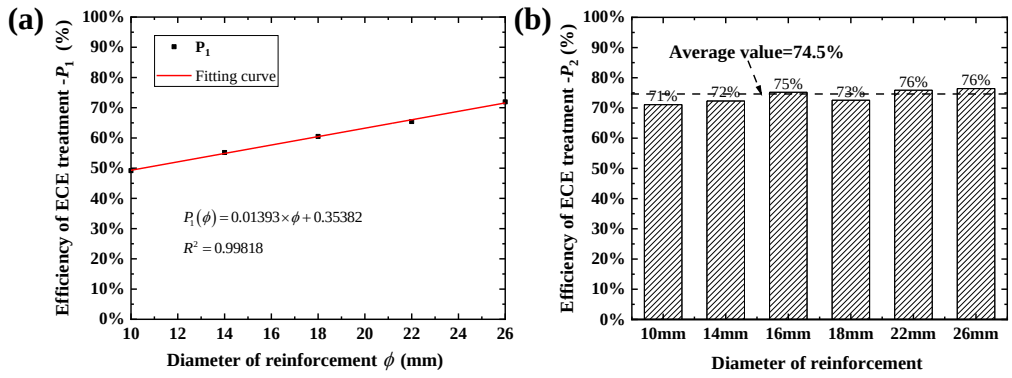

Fig. 22. Comparison of the influence of different reinforcement diameters on the efficiency indexes of ECE treatment. (a) The efficiency index P_1 of ECE treatment, (b) the efficiency index P_2 of ECE treatment.

5.3.3 Thickness of concrete protective cover

The concrete protective cover thickness is stipulated in detail in the Code for durability Design of concrete structures [68], and different structures have different requirements for the minimum thickness of concrete protective cover. For examples, for a harbor wharf with a designed service life of 50 years, it is stipulated that the minimum thickness of the concrete protective cover should be 50 mm. While, for construction projects far away from the marine environment, the required minimum thickness of concrete protective cover is only 30 mm. Therefore, it is necessary to investigate the influence of the thickness of concrete protective cover on the ECE treatment.

In order to illustrate the influence of the thickness of concrete protective cover on the ECE treatment, it is necessary to simulate the ECE treatment of concrete with different concrete protective cover thicknesses. The thickness of the concrete protective cover is from 30 mm to 50 mm with a step of 5 mm, the diameter of reinforcement is 16 mm, and the current density is 2 A/m^2. When the free chloride concentration on the surface of the reinforcement reaches the critical chloride concentration (33.8mol/m^3), the chloride from concrete will be removed by ECE treatment. According the theory of chloride ingress described in section 2.1, the chloride ingress time of concrete with different thickness of the concrete protective cove are calculated when the free chloride concentration on the surface of the reinforcement reaches the critical chloride concentration, as shown in Fig. 23. It can be seen from Fig. 23 that the chloride ingress time corresponding to the critical chloride concentration increases exponentially with the increase of the concrete protective cover thickness. The thicker the concrete protective cover, the longer the service life of the RC structure.

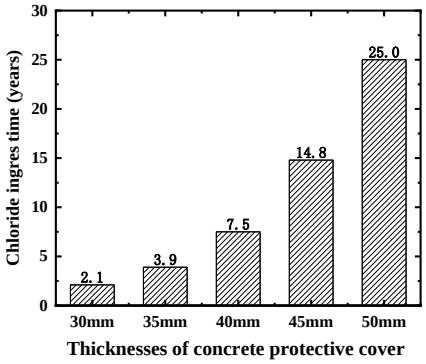

Fig. 23. Chloride ingress time corresponding to the critical chloride concentration for different thicknesses of concrete protective cover.

It is clearly from Fig. 24a that with increasing of ECE treatment time, the ECE treatment efficiency index P_1 with different concrete protective cover thicknesses increases gradually. Additionally, the curves of ECE treatment efficiency index P_1 for 45 mm and 50 mm concrete protective cover are very close. This manifest that the influence of concrete protective cover thickness on the efficiency index P_1 of ECE treatment can be ignored when the thickness of concrete protective cover is more than 45 mm. Furthermore, with the increase of the thickness of the concrete protective cover, the efficiency index P_1 of ECE treatment after 8 weeks of ECE treatment gradually decreases and tends to be stable, as plotted in Fig. 24b. Similar phenomenon have also been observed from the experimental results of Garbacz *et al.* [70]. To express the quantitative relationship between thickness of the concrete protective cover and the ECE treatment efficiency index P_1, we obtain the following fitting formula model through nonlinear analysis:

$$P_1(C) = 7.113 \times C^{-0.625} \tag{20}$$

where C is the thickness of concrete protective cover (mm).

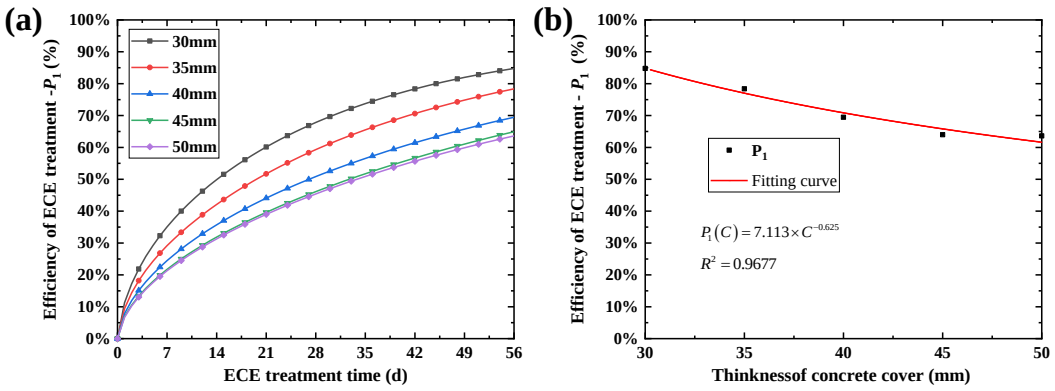

Fig. 24. The profiles of ECE treatment efficiency index P_1. (a) Comparison of the influence of different thicknesses of concrete protective cover on the ECE treatment efficiency index P_1. (b) The relationship between thickness of concrete protective cover and ECE treatment efficiency index P_1 after 8 weeks ECE treatment.

What can be clearly seen from Fig. 25a is that with increasing of ECE treatment time, the ECE treatment efficiency index P_2 with different thicknesses of concrete protective cover also gradually increases. However, the curves of ECE treatment efficiency index P_2 with different thicknesses of concrete protective cover are very close, which indicates that the thickness of concrete protective cover has slight effect on P_2. Fig. 25b demonstrates the histogram of the efficiency index P_2 of ECE treatment for different thicknesses of concrete protective cover after 8 weeks of ECE treatment.

Obviously, the difference of P_2 between the maximum value and the minimum value is only 2%, which is very small and can be ignored.

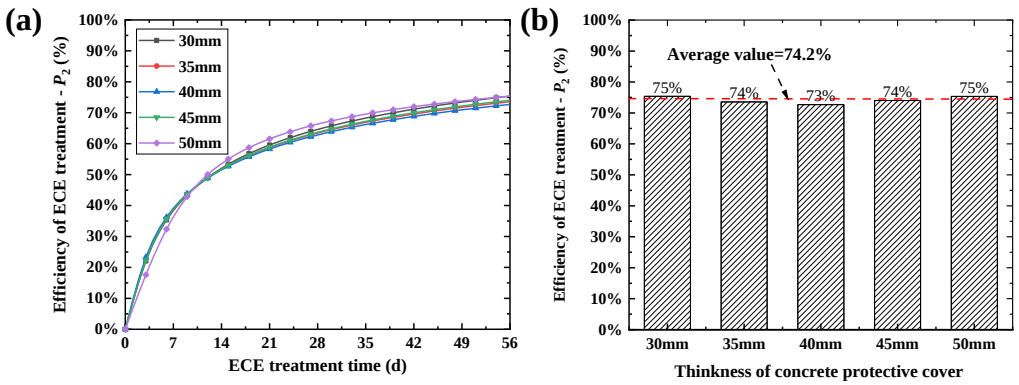

Fig. 25. The profiles of ECE treatment efficiency index P_2. (a) Comparison of different thicknesses of concrete protective cover on the efficiency index P_2 of ECE treatment. (b) The histogram of the efficiency index P_2 of ECE treatment after 8 weeks ECE treatment.

6 Engineering application

The above two-dimensional multi-phase mesoscopic numerical presents a detailed and clear picture of the transport of chloride in the process of chloride ingress and subsequent ECE treatment. In this section, a three-dimensional numerical model is established to simulate the chloride ingress and subsequent ECE treatment process for actual ocean engineering. Fig. 26a provides a corrosion picture of concrete column[71], which shows the corrosion damage caused by chloride ingress in marine engineering. And a geometric model including stress reinforcements and stirrups is established, as shown in Fig. 26b. In order to reduce the computational time of numerical simulation, two basic units are selected as the research object. And the cylindrical reinforcements are simplified to cuboid reinforcements with the same cross-sectional area[22], as shown in Fig. 26c. The diameters of the reinforcements are 16 mm, the thickness of concrete protective cover is 50 mm, and the current density on the surface of reinforcement is 2 A/m^2. Specially, the stirrups are considered in the simulations, and the diameters of the stirrups are 10 mm. In addition, the ECE treatment method is adopted to remove chloride from concrete when the chloride concentration around the surface of reinforcement reaches the critical chloride concentration.

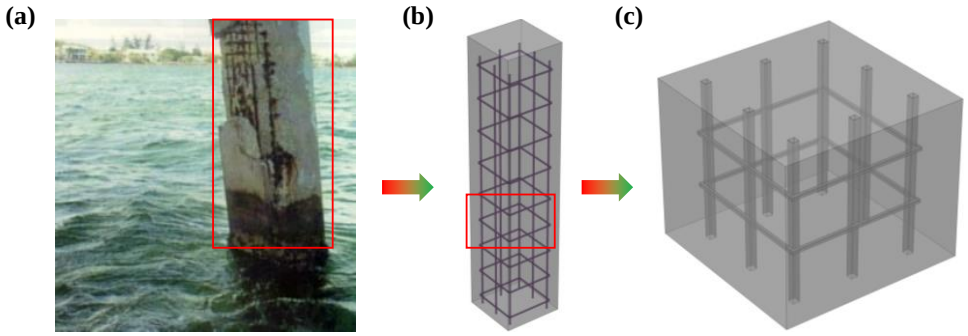

Fig. 26. 3D geometric model schematics of ECE treatment. (a) Reinforced concrete column in marine environment [71]. (b) Finite element geometric model. (c) Representative units.

The distributions of chloride concentration in the z = 100 mm plane and z = 250 mm plane before ECE treatment and after 8 weeks of ECE treatment are demonstrated in Fig. 27 a-e. Compared with free chloride concentration before treatment (Fig. 27 b and d), the free chloride concentration after 8 weeks of ECE treatment is significantly lower (Fig. 27 c and e). This indicates that ECE treatment is a good non-destructive repair method for chloride removal. In practical engineering, in order to avoid damage to the concrete structure, the reinforcing steel with the protective layer falling off due to corrosion is generally used to connect with the cathode, without artificial damage to the reinforced concrete structure. Furthermore, the angle reinforcements are more severely corroded by chloride compared with the middle reinforcements, as shown the Fig. 27b and d. This is mainly due to that the angle reinforcements are corroded in both x and y directions, while the middle reinforcements are corroded only is one direction (*i.e.*, x-direction or y-direction). Similar results have also been obtained from experimental researches conducted by Chang *et al.* [66]. In addition, the concentration of free chloride in the cross-section plane with stirrups (z = 100 mm) is significantly lower than that in the cross-section plane without stirrups (z = 250 mm) after 8 weeks of ECE treatment, as shown in Fig. 27c and e. This indicates that the use of stirrup can improve the efficiency of ECE treatment. This can be attribute to that the use of stirrups could generate a potential gradient along the length direction (*i.e.*, z direction) of reinforcement, thus promoting the removal of chloride from the concrete.

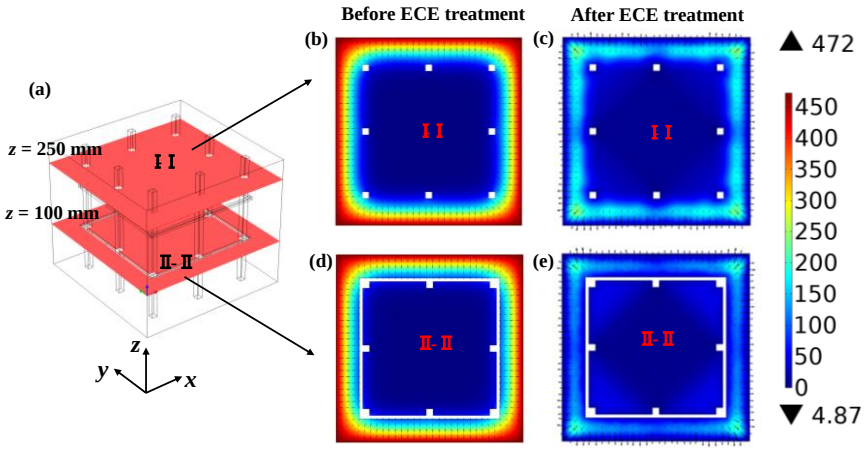

Fig.27. Chloride concentration distribution before and after ECE treatment. (a) Schematic diagram of the cross-sectional position of z = 100 mm and z = 200 mm. (b) Chloride concentration distribution in the cross-section of z = 250 mm before ECE treatment. (c) Chloride concentration distribution in the cross-section of z = 250 mm after 8 weeks ECE treatment. (d) Chloride concentration distribution in the cross-section of z = 100 mm before ECE treatment. (e) Chloride concentration distribution in the cross-section of z = 100 mm after 8 weeks ECE treatment.

In order to quantitatively analyze the effect of ECE treatment, the free chloride concentration profiles along the length direction (*i.e.*, z direction) of reinforcement before treatment and after 8 weeks of ECE treatment are calculated, as demonstrated in Fig. 28. It can be clearly seen from the Fig. 28 that the average concentration of free chloride before repair is 127 mol/m^3, while the average concentration of chloride after 8 weeks of repair is only 49.3 mol/m^3. This indicate the concentration of free chloride in concrete is significantly reduced after ECE treatment. Moreover, the free chloride concentration at the surface of stirrup is the lowest (23 mol/m^3), and the chloride concentration reaches the maximum (58 mol/m^3) at about 20 mm away from the stirrups. This can be owing to

that the stirrup is used as cathodic, and the chloride around stirrup migrates outward under the electric field.

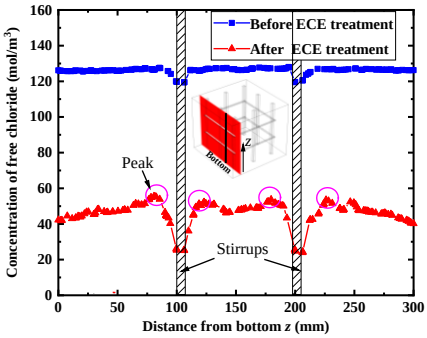

Fig. 28. Concentration profiles of free chloride along the length direction of reinforced concrete column.

7 Conclusions

A multi-phase mesoscopic numerical model is proposed to fully understand the mechanisms of the long-term chloride ingress and the subsequent ECE treatment of RC structure. The influence of key factors (*i.e.*, current density, diameter of reinforcement, and thickness of the concrete protective cover) on the efficiency of ECE treatment is investigated. In addition, the quantitative relationship models between ECE treatment and these factors are established. Finally, a three-dimensional numerical model is developed to simulate the long-term chloride ingress and ECE treatment for actual ocean engineering. Based on a systematic study, the following conclusions can be drawn:

1. The proposed multiphase numerical model presents a detailed and clear picture of the transport of chloride in the process of chloride ingress and the subsequent ECE treatment, providing engineers an effective tool in tackling corrosion problems of RC concrete structures.

2. With the increase of chloride ingress time, if no repair measures are taken, it will inevitably lead to the corrosion of reinforcement. More importantly, the bound chloride concentration will not increase after reaching a stationary value, indicating that the adsorption capacity of concrete decreases with the increase of chloride ingress time.

3. The spatial distributions of free chloride concentration in RC structures changes dramatically after ECE treatment. Additionally, the chloride concentration on the surface of the reinforcement decreases sharply at the initial stage of ECR treatment, and then decreases gradually with the increase of desalting time.

4. The ECE treatment efficiency can be improved by increasing the current density. And the optimized current density is 2 A/m^2. Moreover, the ECE treatment efficiency index P_1 increases linearly, and P_2 first increases and then stabilizes with the increase of current density.

5. The reinforcement diameters has little effect on the ECE treatment efficiency. In addition, the ECE treatment efficiency index P_1 gradually decreases and tends to be stable, while P_2 remains stable with the increase of the thickness of the concrete protective cover.

6. The concentration of free chloride in the cross-section plane with stirrups is significantly lower than that in the cross-section plane without stirrups after ECE treatment. And the free chloride concentration on the surface of stirrup is the lowest.

Author Contributions:

Xuandong Chen: Data curation, Writing, Conceptualization, Methodology, Software, Investigation. **Feng Fu:** Writing- Reviewing and Editing; **Hai Wang**: Writing- Reviewing and Editing, Supervision; **Qiuqun Liang**: Writing- Original draft preparation, Writing- Reviewing and Editing, Investigation. **Aiping Yu**: Software, Data curation. **Kai Qian**: Methodology, Software. **Ping Chen**: Validation, Software.

Acknowledgements:

Authors appreciate the financial supports from the National Natural Science Foundation of China (No. 51968014), Guangxi Key Laboratory of New Energy and Building Energy Saving Foundation (No. 19-J-21-17, 19-J-21-30), and Guangxi Universities Scientific Research Project (2020KY06029), Natural Science Foundation of Guangxi Province (No. 2018GXNSFAA138199), Ph.D. research startup foundation of Guilin University of Technology (No. 002401003523).

Conflicts of Interest: The authors declare no conflict of interest.

References

[1] Y. Ji, Y. Hu, L. Zhang, Z. Bao, Laboratory studies on influence of transverse cracking on chloride-induced corrosion rate in concrete, Cem. Concr. Compos. 69 (2016) 28–37. https://doi.org/10.1016/j.cemconcomp.2015.12.006.

[2] C. Boschmann Käthler, U.M. Angst, A.M. Aguilar, B. Elsener, A systematic data collection on chloride-induced steel corrosion in concrete to improve service life modelling and towards understanding corrosion initiation, Corros. Sci. 157 (2019) 331–336. https://doi.org/10.1016/j.corsci.2019.06.008.

[3] X. Shi, N. Xie, K. Fortune, J. Gong, Durability of steel reinforced concrete in chloride environments: An overview, Constr. Build. Mater. 30 (2012) 125–138. https://doi.org/10.1016/j.conbuildmat.2011.12.038.

[4] J. Xia, Q. feng Liu, J. hong Mao, Z. hai Qian, S. jie Jin, J. yuan Hu, W. liang Jin, Effect of environmental temperature on efficiency of electrochemical chloride removal from concrete, Constr. Build. Mater. 193 (2018) 189–195. https://doi.org/10.1016/j.conbuildmat.2018.10.187.

[5] K. Krabbenhøft, J. Krabbenhøft, Application of the Poisson-Nernst-Planck equations to the migration test, Cem. Concr. Res. 38 (2008) 77–88. https://doi.org/10.1016/j.cemconres.2007.08.006.

[6] B. Johannesson, K. Yamada, L.O. Nilsson, Y. Hosokawa, Multi-species ionic diffusion in concrete with account to interaction between ions in the pore solution and the cement hydrates, Mater. Struct. Constr. 40 (2007) 651–665. https://doi.org/10.1617/s11527-006-9176-y.

[7] E. Samson, J. Marchand, Modeling the transport of ions in unsaturated cement-based materials, Comput. Struct. 85 (2007) 1740–1756. https://doi.org/10.1016/j.compstruc.2007.04.008.

[8] Y. Tian, Z. Tian, N. Jin, X. Jin, W. Yu, A multiphase numerical simulation of chloride ions diffusion in concrete using electron microprobe analysis for characterizing properties of ITZ, Constr. Build. Mater. 178 (2018) 432–444. https://doi.org/10.1016/j.conbuildmat.2018.05.047.

[9] J. Peng, S. Hu, J. Zhang, C.S. Cai, L. yuan Li, Influence of cracks on chloride diffusivity in concrete: A five-phase mesoscale model approach, Constr. Build. Mater. 197 (2019) 587–596. https://doi.org/10.1016/j.conbuildmat.2018.11.208.

[10] H. Ye, Y. Tian, N. Jin, X. Jin, C. Fu, Influence of cracking on chloride diffusivity and moisture influential depth in concrete subjected to simulated environmental conditions, Constr. Build. Mater. 47 (2013) 66–79. https://doi.org/10.1016/j.conbuildmat.2013.04.024.

[11] T. Ueda, K. Wakitani, A. Nanasawa, Influence of electrolyte temperature on efficiency of electrochemical chloride removal from concrete, Electrochim. Acta. 86 (2012) 23–27. https://doi.org/10.1016/j.electacta.2012.05.026.

[12] H. Chu, B. Zhang, S. Zhao, M. Guo, Y. Liang, L. Jiang, Z. Song, Effect of electric current on the stability of bound chloride, Cem. Concr. Compos. 103 (2019) 71–79. https://doi.org/10.1016/j.cemconcomp.2019.04.015.

[13] N.M. Ihekwaba, B.B. Hope, C.M. Hansson, Carbonation and electrochemical chloride extraction from concrete, Cem. Concr. Res. 26 (1996) 1095–1107. https://doi.org/10.1016/0008-8846(96)00076-2.

[14] L.Y. Li, C.L. Page, Modelling of electrochemical chloride extraction from concrete: Influence of ionic activity coefficients, Comput. Mater. Sci. 9 (1998) 303–308. https://doi.org/10.1016/s0927-0256(97)00152-3.

[15] L.Y. Li, C.L. Page, Finite element modelling of chloride removal from concrete by an electrochemical method, Corros. Sci. 42 (2000) 2145–2165. https://doi.org/10.1016/S0010-938X(00)00044-5.

[16] Y. Wang, L.Y. Li, C.L. Page, A two-dimensional model of electrochemical chloride removal from concrete, Comput. Mater. Sci. 20 (2001) 196–212. https://doi.org/10.1016/S0927-0256(00)00177-4.

[17] C. Andrade, J.M. Diez, A. Alamán, C. Alonso, Mathematical modelling of electrochemical chloride extraction from concrete, Cem. Concr. Res. 25 (1995) 727–740. https://doi.org/10.1016/0008-8846(95)00063-I.

[18] J.C. Orellan, G. Escadeillas, G. Arliguie, Electrochemical chloride extraction: Efficiency and side effects, Cem. Concr. Res. 34 (2004) 227–234. https://doi.org/10.1016/j.cemconres.2003.07.001.

[19] Y. Liu, X. Shi, Cathodic protection technologies for reinforced concrete: Introduction and recent developments, Rev. Chem. Eng. 25 (2009) 339–388. https://doi.org/10.1515/REVCE.2009.25.5-6.339.

[20] A. Pérez, M.A. Climent, P. Garcés, Electrochemical extraction of chlorides from reinforced concrete using a conductive cement paste as the anode, Corros. Sci. 52 (2010) 1576–1581. https://doi.org/10.1016/j.corsci.2010.01.016.

[21] J. Xu, F. Li, Numerical analysis on efficiency of electrochemical chloride extraction of one side anode in concrete, Ocean Eng. 179 (2019) 38–50. https://doi.org/10.1016/j.oceaneng.2019.03.018.

[22] J. Xia, X. Cheng, Q. feng Liu, H. bo Xie, X. ping Zhong, S. jie Jin, J. hong Mao, W. liang Jin, Effect of the stirrup on the transport of chloride ions during electrochemical chloride removal in concrete structures, Constr. Build. Mater. 250 (2020) 118898. https://doi.org/10.1016/j.conbuildmat.2020.118898.

[23] J. Orlikowski, S. Cebulski, K. Darowicki, Electrochemical investigations of conductive coatings applied as anodes in cathodic protection of reinforced concrete, Cem. Concr. Compos. 26 (2004) 721–728. https://doi.org/10.1016/S0958-9465(03)00105-7.

[24] R.B. Polder, G. Leegwater, D. Worm, W. Courage, Service life and life cycle cost modelling of cathodic protection systems for concrete structures, Cem. Concr. Compos. 47 (2014) 69–74. https://doi.org/10.1016/j.cemconcomp.2013.05.004.

[25] W. Guo, J. Hu, Y. Ma, H. Huang, S. Yin, J. Wei, Q. Yu, The application of novel lightweight functional aggregates on the mitigation of acidification damage in the external anode mortar during cathodic protection for reinforced concrete, Corros. Sci. 165 (2020) 108366. https://doi.org/10.1016/j.corsci.2019.108366.

[26] P. Pedeferri, Cathodic protection and cathodic prevention, Constr. Build. Mater. 10 (1996) 391–402. https://doi.org/10.1016/0950-0618(95)00017-8.

[27] B. Elsener, M. Molina, H. Böhni, The electrochemical removal of chlorides from reinforced concrete, Corros. Sci. 35 (1993). https://doi.org/10.1016/0010-938X(93)90385-T.

[28] R.N. Swamy, S. McHugh, Effectiveness and structural implications of electrochemical chloride extraction from reinforced concrete beams, Cem. Concr. Compos. 28 (2006) 722–733. https://doi.org/10.1016/j.cemconcomp.2006.05.012.

[29] G. Fajardo, G. Escadeillas, G. Arliguie, Electrochemical chloride extraction (ECE) from steel-reinforced concrete specimens contaminated by "artificial" sea-water, Corros. Sci. 48 (2006) 110–125. https://doi.org/10.1016/j.corsci.2004.11.015.

[30] P. Garcés, M.J. Sánchez De Rojas, M.A. Climent, Effect of the reinforcement bar arrangement on the efficiency of electrochemical chloride removal technique applied to reinforced concrete structures, Corros. Sci. 48 (2006) 531–545. https://doi.org/10.1016/j.corsci.2005.02.010.

[31] W. Yeih, J.J. Chang, C.C. Chang, K.L. Chen, M.C. Chi, Electrochemical chloride removal for reinforced concrete with steel rebar cage using auxiliary electrodes, Cem. Concr. Compos. 74 (2016) 136–146. https://doi.org/10.1016/j.cemconcomp.2016.08.002.

[32] M. Zhang, G. Ye, K. Van Breugel, Multiscale lattice Boltzmann-finite element modelling of chloride diffusivity in cementitious materials. Part II: Simulation results and validation, Mech. Res. Commun. 58 (2014) 64–72. https://doi.org/10.1016/j.mechrescom.2014.01.001.

[33] Q.F. Liu, J. Xia, D. Easterbrook, J. Yang, L.Y. Li, Three-phase modelling of electrochemical chloride removal from corroded steel-reinforced concrete, Constr. Build. Mater. 70 (2014) 410–427. https://doi.org/10.1016/j.conbuildmat.2014.08.003.

[34] M. Castellote, C. Andrade, C. Alonso, Electrochemical removal of chlorides - modelling of the extraction, resulting profiles and determination of the efficient time of treatment, Cem. Concr. Res. 30 (2000) 615–621. https://doi.org/10.1016/S0008-8846(00)00220-9.

[35] Q. feng Liu, L.Y. Li, D. Easterbrook, J. Yang, Multi-phase modelling of ionic transport in concrete when subjected to an externally applied electric field, Eng. Struct. 42 (2012) 201–213. https://doi.org/10.1016/j.engstruct.2012.04.021.

[36] V. Baroghel-Bouny, X. Wang, M. Thiery, M. Saillio, F. Barberon, Prediction of chloride binding isotherms of cementitious materials by "analytical" model or "numerical" inverse analysis, Cem. Concr. Res. 42 (2012) 1207–1224. https://doi.org/10.1016/j.cemconres.2012.05.008.

[37] D. Li, L. yuan Li, X. Wang, Chloride diffusion model for concrete in marine environment with considering binding effect, Mar. Struct. 66 (2019) 44–51. https://doi.org/10.1016/j.marstruc.2019.03.004.

[38] V.Q. Tran, A. Soive, V. Baroghel-Bouny, Modelisation of chloride reactive transport in concrete including thermodynamic equilibrium, kinetic control and surface complexation, Cem. Concr. Res. 110 (2018) 70–85. https://doi.org/10.1016/j.cemconres.2018.05.007.

[39] W. qiang Jiang, X. han Shen, S. Hong, Z. yan Wu, Q. feng Liu, Binding capacity and diffusivity of concrete subjected to freeze-thaw and chloride attack: A numerical study, Ocean Eng. 186 (2019) 106093. https://doi.org/10.1016/j.oceaneng.2019.05.075.

[40] T. Ishida, P.O.N. Iqbal, H.T.L. Anh, Modeling of chloride diffusivity coupled with non-linear binding capacity in sound and cracked concrete, Cem. Concr. Res. 39 (2009) 913–923. https://doi.org/10.1016/j.cemconres.2009.07.014.

[41] M. Fenaux, E. Reyes, J.C. Gálvez, A. Moragues, Modelling the transport of chloride and other ions in cement-based materials, Cem. Concr. Compos. 97 (2019) 33–42. https://doi.org/10.1016/j.cemconcomp.2018.12.009.

[42] P.T. Nguyen, O. Amiri, Study of electrical double layer effect on chloride transport in unsaturated concrete, Constr. Build. Mater. 50 (2014) 492–498. https://doi.org/10.1016/j.conbuildmat.2013.09.013.

[43] Z. Pan, A. Chen, X. Ruan, Spatial variability of chloride and its influence on thickness of concrete cover: A two-dimensional mesoscopic numerical research, Eng. Struct. 95 (2015) 154–169. https://doi.org/10.1016/j.engstruct.2015.03.061.

[44] D. Li, X. Wang, L. yuan Li, An analytical solution for chloride diffusion in concrete with considering binding effect, Ocean Eng. 191 (2019) 106549. https://doi.org/10.1016/j.oceaneng.2019.106549.

[45] Q. feng Liu, G. lin Feng, J. Xia, J. Yang, L. yuan Li, Ionic transport features in concrete composites containing various shaped aggregates: a numerical study, Compos. Struct. 183 (2018) 371–380. https://doi.org/10.1016/j.compstruct.2017.03.088.

[46] Y. Hosokawa, K. Yamada, B. Johannesson, L.O. Nilsson, Development of a multi-species mass transport model for concrete with account to thermodynamic phase equilibriums, Mater. Struct. Constr. 44 (2011) 1577–1592. https://doi.org/10.1617/s11527-011-9720-2.

[47] V.Q. Tran, A. Soive, S. Bonnet, A. Khelidj, A numerical model including thermodynamic equilibrium, kinetic control and surface complexation in order to explain cation type effect on chloride binding capability of concrete, Constr. Build. Mater. 191 (2018) 608–618. https://doi.org/10.1016/j.conbuildmat.2018.10.058.

[48] P. Spiesz, M.M. Ballari, H.J.H. Brouwers, RCM: A new model accounting for the non-linear chloride binding isotherm and the non-equilibrium conditions between the free- and bound-chloride concentrations, Constr. Build. Mater. 27 (2012) 293–304. https://doi.org/10.1016/j.conbuildmat.2011.07.045.

[49] B. Elsener, U. Angst, Mechanism of electrochemical chloride removal, Corros. Sci. 49 (2007) 4504–4522. https://doi.org/10.1016/j.corsci.2007.05.019.

[50] K.B. Kim, J.P. Hwang, K.Y. Ann, Influence of cementitious binder on chloride removal under electrochemical treatment in concrete, Constr. Build. Mater. 104 (2016) 191–197. https://doi.org/10.1016/j.conbuildmat.2015.12.052.

[51] A. Toumi, R. François, O. Alvarado, Experimental and numerical study of electrochemical chloride removal from brick and concrete specimens, Cem. Concr. Res. 37 (2007) 54–62. https://doi.org/10.1016/j.cemconres.2006.09.012.

[52] L.S. Selwyn, W.R. McKinnon, V. Argyropoulos, Models for chloride ion diffusion in archaeological iron, Stud. Conserv. 46 (2001) 109–120. https://doi.org/10.2307/1506841.

[53] G.L. Feng, L.Y. Li, B. Kim, Q.F. Liu, Multiphase modelling of ionic transport in cementitious materials with surface charges, Comput. Mater. Sci. 111 (2016) 339–349. https://doi.org/10.1016/j.commatsci.2015.09.060.

[54] J. Xia, L.Y. Li, Numerical simulation of ionic transport in cement paste under the action of externally applied electric field, Constr. Build. Mater. 39 (2013) 51–59. https://doi.org/10.1016/j.conbuildmat.2012.05.036.

[55] L. Wu, W. Li, X. Yu, Time-dependent chloride penetration in concrete in marine environments, Constr. Build. Mater. 152 (2017) 406–413. https://doi.org/10.1016/j.conbuildmat.2017.07.016.

[56] J. van Brakel, P.M. Heertjes, Analysis of diffusion in macroporous media in terms of a porosity, a tortuosity and a constrictivity factor, Int. J. Heat Mass Transf. 17 (1974) 1093–1103. https://doi.org/10.1016/0017-9310(74)90190-2.

[57] L. Jin, W. Yu, D. Li, X. Du, Numerical and theoretical investigation on the size effect of concrete compressive strength considering the maximum aggregate size, Int. J. Mech. Sci. 192 (2021) 106130. https://doi.org/10.1016/j.ijmecsci.2020.106130.

[58] H.W. Walraven, J. C， Reinhardt, Theory and Experiments on the Mechanical Behaviour of Cracks in Plain and Reinforced Concrete Subjected to Shear Loading, HERON. 26(1A) (1981) 26–39.

[59] X. Chen, A. Yu, G. Liu, P. Chen, Q. Liang, A multi-phase mesoscopic simulation model for the diffusion of chloride in concrete under freeze–thaw cycles, Constr. Build. Mater. 265 (2020) 120223. https://doi.org/10.1016/j.conbuildmat.2020.120223.

[60] P. Zhang, Y. Cong, M. Vogel, Z. Liu, H.S. Müller, Y. Zhu, T. Zhao, Steel reinforcement corrosion in concrete under combined actions: The role of freeze-thaw cycles, chloride ingress, and surface impregnation, Constr. Build. Mater. 148 (2017) 113–121. https://doi.org/10.1016/j.conbuildmat.2017.05.078.

[61] W. Li, L. Guo, A mechanical-diffusive peridynamics coupling model for meso-scale simulation of chloride penetration in concrete under loadings, Constr. Build. Mater. 241 (2020) 118021. https://doi.org/10.1016/j.conbuildmat.2020.118021.

[62] W. qiang Jiang, X. han Shen, J. Xia, L. xuan Mao, J. Yang, Q. feng Liu, A numerical study on chloride diffusion in freeze-thaw affected concrete, Constr. Build. Mater. 179 (2018) 553–565. https://doi.org/10.1016/j.conbuildmat.2018.05.209.

[63] A. Pachón-Montaño, J. Sánchez-Montero, C. Andrade, J. Fullea, E. Moreno, V. Matres, Threshold concentration of chlorides in concrete for stainless steel reinforcement: Classic austenitic and new duplex stainless steel, Constr. Build. Mater. 186 (2018) 495–502. https://doi.org/10.1016/j.conbuildmat.2018.07.081.

[64] Y. Cao, C. Gehlen, U. Angst, L. Wang, Z. Wang, Y. Yao, Critical chloride content in reinforced concrete — An updated review considering Chinese experience, Cem. Concr. Res. 117 (2019) 58–68. https://doi.org/10.1016/j.cemconres.2018.11.020.

[65] S. Jones, N. Martys, Y. Lu, D. Bentz, Simulation studies of methods to delay corrosion and increase service life for cracked concrete exposed to chlorides, Cem. Concr. Compos. 58 (2015) 59–69. https://doi.org/10.1016/j.cemconcomp.2014.12.014.

[66] C.C. Chang, W. Yeih, J.J. Chang, R. Huang, Effects of stirrups on electrochemical chloride removal efficiency, Constr. Build. Mater. 68 (2014) 692–700. https://doi.org/10.1016/j.conbuildmat.2014.06.091.

[67] V. Saraswathy, H.S. Lee, S. Karthick, S.J. Kwon, Extraction of chloride from chloride contaminated concrete through electrochemical method using different anodes, Constr. Build. Mater. 158 (2018) 549–562. https://doi.org/10.1016/j.conbuildmat.2017.10.052.

[68] Y. Wang, C. Liu, Q. Li, L. Wu, Chloride ion concentration distribution characteristics within concrete covering-layer considering the reinforcement bar presence, Ocean Eng. 173 (2019) 608–616. https://doi.org/10.1016/j.oceaneng.2019.01.048.

[69] Y. Wang, X. Gong, L. Wu, Prediction model of chloride diffusion in concrete considering the coupling effects of coarse aggregate and steel reinforcement exposed to marine tidal environment, Constr. Build. Mater. 216 (2019) 40–57. https://doi.org/10.1016/j.conbuildmat.2019.04.221.

[70] A. Garbacz, M. Górka, L. Courard, Effect of concrete surface treatment on adhesion in repair systems, Mag. Concr. Res. 57 (2005) 49–60. https://doi.org/10.1680/macr.2005.57.1.49.

[71] X. han Shen, Q. feng Liu, Z. Hu, W. qiang Jiang, X. Lin, D. Hou, P. Hao, Combine ingress of chloride and carbonation in marine-exposed concrete under unsaturated environment: A numerical study, Ocean Eng. 189 (2019) 106350. https://doi.org/10.1016/j.oceaneng.2019.106350.